Analysis of fan-stage gap flow data generated using an LBM/VLES method

Sheryl Grace *
Dept. of Mechanical Engineering
Boston University, Boston, MA 02215

Ignacio Gonzalez-Martino †
Dassault Systemes, 76 route de la Demi-Lune, Paris F-92057, France

Damiano Casalino, ‡
Dept. of Aerodynamics, Wind Energy, Flight Performance and Propulsion
Delft University of Technology, 2629 HS Delft, The Netherlands

Quantitative analysis of the simulated flow field in the gap between the fan and fan exit guide vane (FEGV) computed with the Lattice Boltzmann based software PowerFLOW for two different vane configurations and two solution methods is presented. One simulation used a coarser mesh near the rotor and a trip to trigger turbulent transition on the rotor. The other simulation did not rely on a trip but employed a much finer mesh near the rotor. The study compares the results of the simulations with experimental measurements to assess the mean flow, the turbulence intensity and the turbulence length scale. The research reported in this paper is a continuation of that discussed in a previous paper.[1] The two computational methods led to slight differences in the turbulence intensity and turbulence length scale but not as large effect as was originally anticipated. As well, the simulation without the turbulence transition trip on the rotor significantly underpredicts the turbulence intensity. Both simulation methods predict much larger turbulence length scales than were measured. The lengthscale is calculated mutliple ways using the simulated data and all methods are in agreement. The turbulent velocity spectrum is analyzed and the ability for models such as Liepmann and Gauss to reconstruct it is assessed. Finally, the predicted acoustic power in the exhaust duct obtained from a low-order acoustic method with the simulated flow parameters used as input is provided. The results highlight the role the turbulent length scale plays in the acoustic prediction.

I. Introduction

Interaction noise due to rotor wake flow through a fan exit guide vane (FEGV) in the fan stage of a turbofan engine leads to both tonal and broadband noise. Of interest in this paper is the prediction of the broadband noise. Many simulation methods have been proposed for predicting the broadband noise. Recently, full flow and noise simulations have been presented based on a very large eddy simulation method (VLES) and the Ffowcs-Williams and Hawkings Equation.[2] Other methods that focus solely on the noise

*Associate Professor, AIAA Associate Fellow
†AIAA Member.
‡Professor, AIAA Member

produced by the rotor-wake interaction with the stator utilize a two-step approach in which the wake turbulence is modeled computationally or obtained via experiment as a first step and then the interaction of the turbulence with the FEGV is considered as a second step. For both methods, accurate broadband noise prediction relies on on accurate prediction of fan wake turbulence quantities. As such this paper, analyzes the flow predicted by the VLES with a focus on the important turbulent quantities. The VLES has been performed via PowerFLOW and flow data inbetween the rotor and stator have been stored for every 16th time step over 10 fan revolutions. Therefore, the velocity time traces can be analyzed exactly as the experimental hotwire data are analyzed The Source Diagnostic Test (SDT) performed by NASA in the late 90s provides a benchmarking platform for simulations of fan noise.[3,4,5,6] The baseline and low noise vane configurations from the SDT at the approach rotor speed are considered in the present work. The baseline vane case was run using a coarser mesh near the rotor and a trip to trigger turbulent transition on the rotor. The low noise confirmation case does not rely on a trip and employs a much finer mesh near the rotor. Previous analysis of the baseline vane configuration simulated with the trip showed that the turbulence length scale was overpredicted and the mean wake deficit was underpredicted. Comparison with the new simulation allow for assessment of the influence of the trip as well as an investigation of the influence of the FEGV on its inflow. This paper provides a quantitative analysis of the mean and turbulent flow quantities computed with PowerFLOW. The quantities of interest and methods for acquiring them from time resolved velocity data are described in Ref. [7] and utilized in Refs. [8,9] and were used in the previous related study.[1]

II. SDT configuration and computational setup

Fig. 1 illustrates the SDT fan rig with the the low-noise vane. The geometry is perfectly axisymmetric. The rotor radius is 10.97 in, the bypass exhaust radius is 10.66 in and the lip intake radius is 11.66 in.The rotor consists of 22 blades with a casing/blade-tip gap of about 0.02 in. The Low-Noise vane has 26 swept vanes. The other vane geometry considered in this work is the baseline case. The baseline case has 54

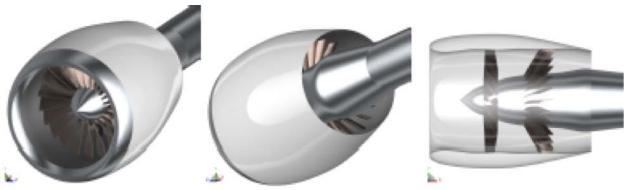

Figure 1: Reference SDT Low-Noise configuration.

smaller unswept vanes. The simulation data included in this work actually utilized a baseline vane with a wavy leading edge. Previously, the effect of the wavy leading edge was shown to be negligible.[1] The gap-flow analysis in this paper uses data from the volume shown in red in Figure 2. At the approach rotor speed, 7808 RPM, both hotwire and laser-doppler velocimetry (LDV) data were acquired. The measurements were taken at two axial locations referred to as Stations 1 and 2 throughout this paper. The first station was placed midway between the rotor and FEGV and the second station was at a location very near where the leading edge of the unswept vane cases which is why the data were acquired using the swept vane. 50 radial locations were used for hotwire measurement. LDV data were acquired at 44 radial positions at station 1 and 45 positions at Station 2. The flow data were originally described and analyzed in Ref. [10].

All simulations reported in this paper have been performed by using, as initial condition, the solution

obtained by using a coarser mesh and achieving an acceptable statistical convergence. The time step is 1.364×10^{-7}s and rotor revolutions are stored after a very short initial transient of three blade passages. The CPU cost is of the order of six thousand CPU hours per rotor revolution using 720 cores Intel Sandybridge 2.7 GHz.

III. Method

A. Mean flow

To analyze the mean flow, both circumferentially averaged and total mean flow values of the flow field at Stations 1 and 2 are considered. When the circumferentially averaged values are plotted, the minimum flow point for the streamwise flow is aligned with the center of the passage at the midspan location. The flow is resolved into its mean streamwise direction and two perpendicular directions labeled upwash and tangential. These flow directions are most often used throughout the paper, however, the mean flow is also projected into the axial and circumferential directions for some comparisons.

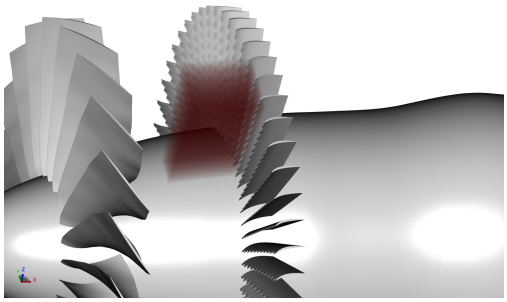

Figure 2: Geometry used in PowerFLOW simulation and volume from which data were extracted and analyzed.

B. Turbulent flow

Gap flow quantities including the turbulence intensity, turbulent kinetic energy, and integral length scale are analyzed in this work. The turbulence intensity is obtained from both the hotwire data and the LBM results by first performing an FFT on the time resolved velocity data. The DC offset and first four tones are removed from the FFT result. An inverse FFT is then performed to obtain the turbulent part of the velocity signal. The turbulent signal is then squared, averaged, and then the square root is taken to obtain an RMS value. The total RMS value at a radial probe location is obtained as well as the circumferentially averaged values. Again, if an average passage value is reported, the peak value of the streamwise component is shifted to the midpassage location at midspan and all other components and spanwise results are shifted by the same amount.

Many methods for obtaining the integral length scale are utilized in this paper. The method that was used by Podboy to obtain the integral length scale from the hotwire data provides is based on Taylor's frozen turbulence hypothesis. It is assumed that the convection of the turbulence can be taken to be entirely due to the mean flow. Hence the flow probes (either physical hotwire or computational data retrievals) will measure the local flow with $x_s = U_s t$ where x_s is distance in the streamwise direction. The streamwise length scales, both longitudinal and transverse, can be obtained then from the time series data as

$$L_{s_i} = \overline{U_s} \int_0^\infty \frac{\overline{u_i'(\tau) u_i'(\tau + t)}}{u_i'^2} dt \tag{1}$$

where i becomes s for streamwise, u for upwash, and t for tangential. L_{s_s} is then the longitudinal length scale and L_{s_u} and L_{s_t} are transverse length scales. In practice, the integration is performed from 0 to the first zero crossing of the integrand.

When data are sampled simultaneously as is the case in a computation, the length scales in other directions can also be considered. For instance, the lengths scales based on radial separation can be considered. In this case

$$L_{r_i} = \int_0^\infty \frac{\overline{u_i'(r) + u_i'(r + \triangle r)}}{u_i'^2} d \triangle r \tag{2}$$

Now, when i is r it refers to the longitudinal length scale and when $i = a$ for axial or c for circumferential it refers to the transverse length scales. Similarly, a second calculation of the streamwise longitudinal and transverse length scales can be obtained by using appropriate data from probes separated along the streamline.

IV. Results

A. Mean flow

The mean flow is analyzed first. As shown in Fig. 2, the simulation data are available circumferentially across one blade passage. Fig. 3 shows the volume from the front as a 2D slice. In the SDT experiment, the hotwire probe was moved along a single radial line to obtain data at different locations between the hub and tip. When analyzing the computational data, a circumferential location for setting the radial line must be selected. As such, it was of of interest to see if radial slices at different circumferential locations from 90° to 106° as shown in Fig. 3 provide different flow values. Fig. 4 shows the streamwise flow determine by radial probes at different circumferential locations at Station 1. For the total mean values, there is no appreciable effect present. However, the calculated average passage wake does vary slightly from circumferential slice to circumferential slice. The variation from slice to slice might be reduced if the grid were perfectly aligned with the wake throughout the entire gap. To account for the difference from slice to slice, the computed wakes shown in this paper are obtained by averaging over the available circumferential slice locations.

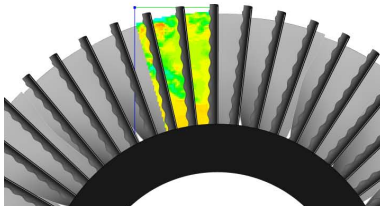

Figure 3: 2D view of data volume.

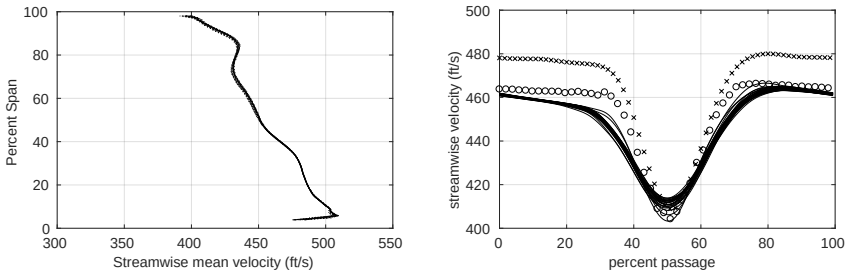

(a) Radial distribution.

(b) Average passage at midspan.

Figure 4: Streamwise mean flow. Station 1. x - hotwire data, o - LDV data, lines - VLES data from different circumferential locations.

The streamwise mean wake measured experimentally with the hotwire (HW) and the laser dopper velocimeter (LDV) is also shown in Fig. 4b. The experimental data are included so that two points can be made. First, the computational results are much closer to the LDV data. This has been noted previously and indeed it has been determined that there was a bias in the SDT hotwire measurements. Second, in order to best compare the wake deficit, a relative velocity which does not contain the total mean value will be used in this paper when plotting the

average passage profiles.

The radial distribution of the total mean velocity at Stations 1 and 2 are shown in Figs 5 and 6. HW denotes the hotwire data, LDV denotes the LDV data, LBM BL denotes the simulation data for the baseline, wavy leading edge, vane using a turbulence transition trip on the rotor blades, and LBM LN denotes the simulation data for the low noise, straight leading edge, vane performed with a finer mesh near the rotor blades and no trip. Except for radial locations very near the hub and casing, the computed total mean flow results for the low noise vane case agree very well with the LDV measurements (there are no radial LDV measurements). The baseline vane case shows greater discrepancies especially at Station 2 where the vanes are very near the probes.

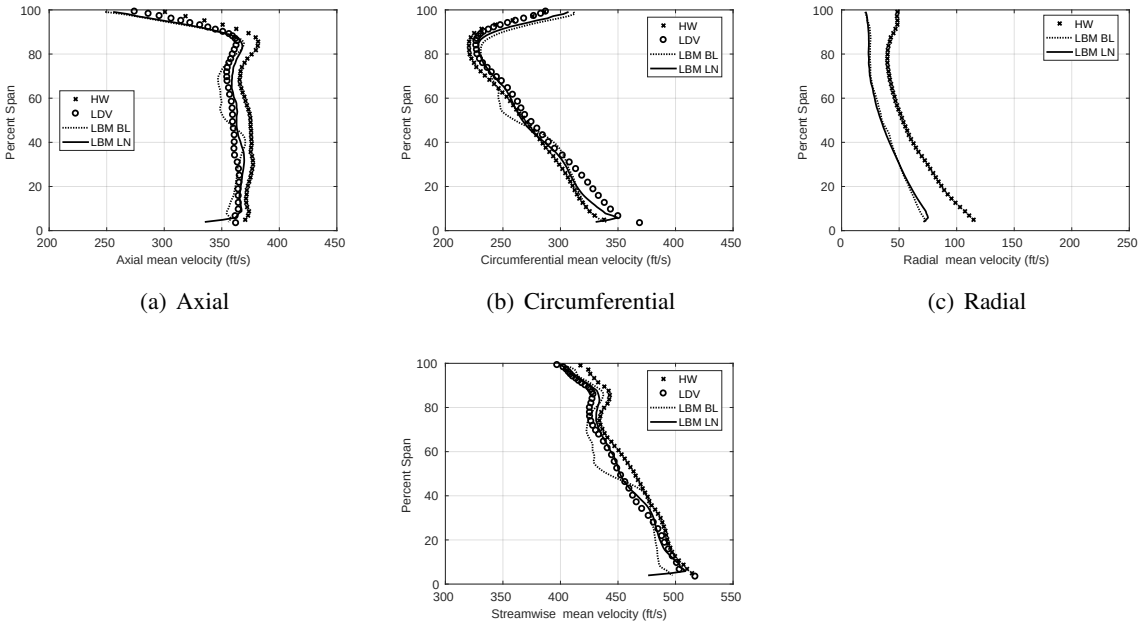

(a) Axial (b) Circumferential (c) Radial

(d) Streamwise

Figure 5: Mean flow velocity vs span location at Station 1.

The mean flow average passage at Stations 1 and 2 are shown in Figs. 7 and 8. Again, it is clear that the simulation without the boundary layer trip that instead uses a refined grid near the blades predicts the mean flow better. When the trip is used in the simulation, it effectively causes extra diffusion as the wake depth is too shallow and width is too large. This is not the case when the finer grid and no trip are utilized. At Station 2 the improvement is even greater, but it is surmised that at this location the low noise configuration contributes to the better agreement with experiment as compared to the baseline vane simulation. The thought that differences arise simply because the computational results provide only 10 rotor revolutions and the experiments included more than 100 revolutions was previously shown to be incorrect by only using 10 revolutions of the experimental data.[1] The results for 10 and 100 revolutions were identical. The results shown in this paper vary slightly from related results presented in.[1] The difference stems from the averaging over the circumferential probe locations in the present work.

The mean flow angle at Station 2 was also recorded in order to pinpoint any potential effect in the baseline vane case. Fig. 9 shows the radial distribution of the mean flow angle taken at different circumferential probe locations in both simulations. The flow angle at a single radial location near midspan is also shown.

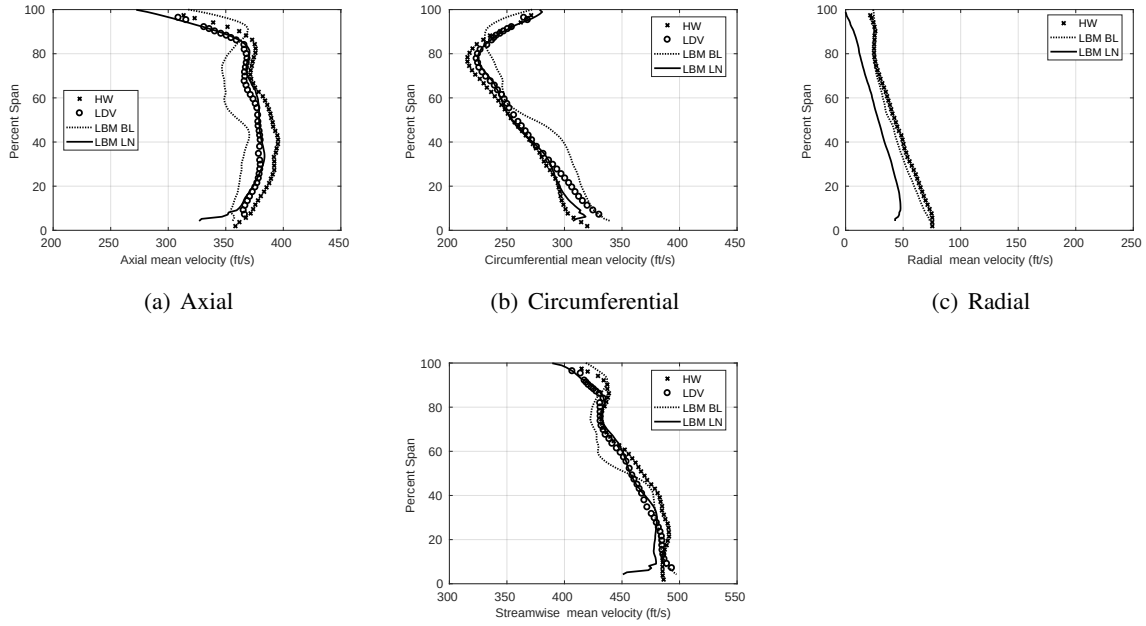

(a) Axial (b) Circumferential (c) Radial

(d) Streamwise

Figure 6: Mean flow velocity vs span location at Station 2.

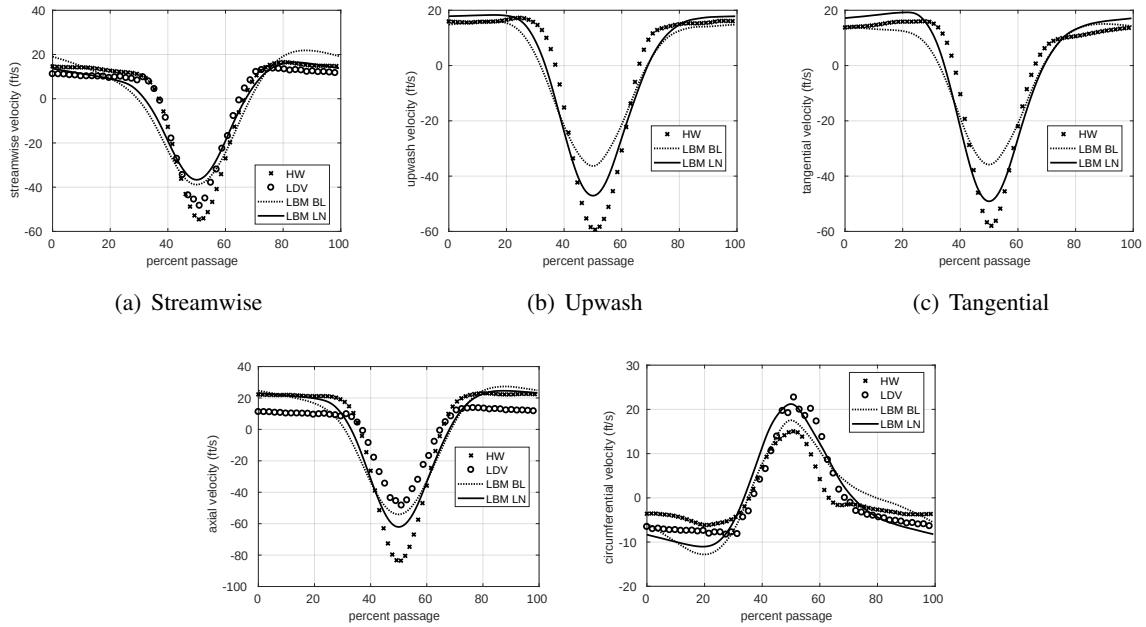

(a) Streamwise (b) Upwash (c) Tangential

(d) Axial (e) Circumferential

Figure 7: Midspan average passage velocity (ft/s) components at Station 1. Total mean subtracted out.

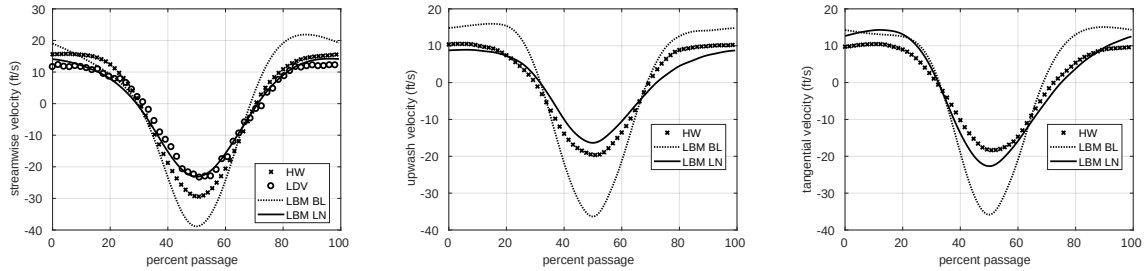

(a) Streamwise

(b) Upwash

(c) Tangential

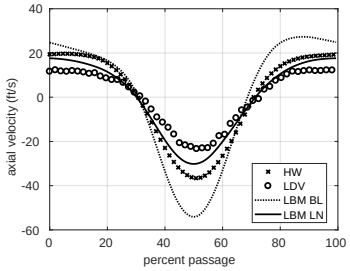

(d) Axial

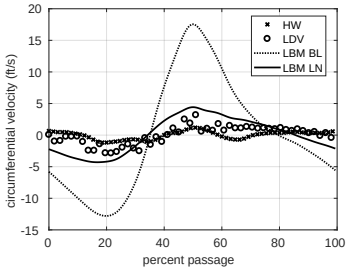

(e) Circumferential

Figure 8: Midspan average passage velocity (ft/s) components at Station 2. Total mean subtracted out.

For the baseline vane, one blade passage encompasses 2.45 vane passages. The slight influence of the baseline vanes on the mean flow is clearly seen. For the low-noise vane configuration in which the vanes are swept downstream and one blade passage is smaller than one vane passage, no potential effect is seen.

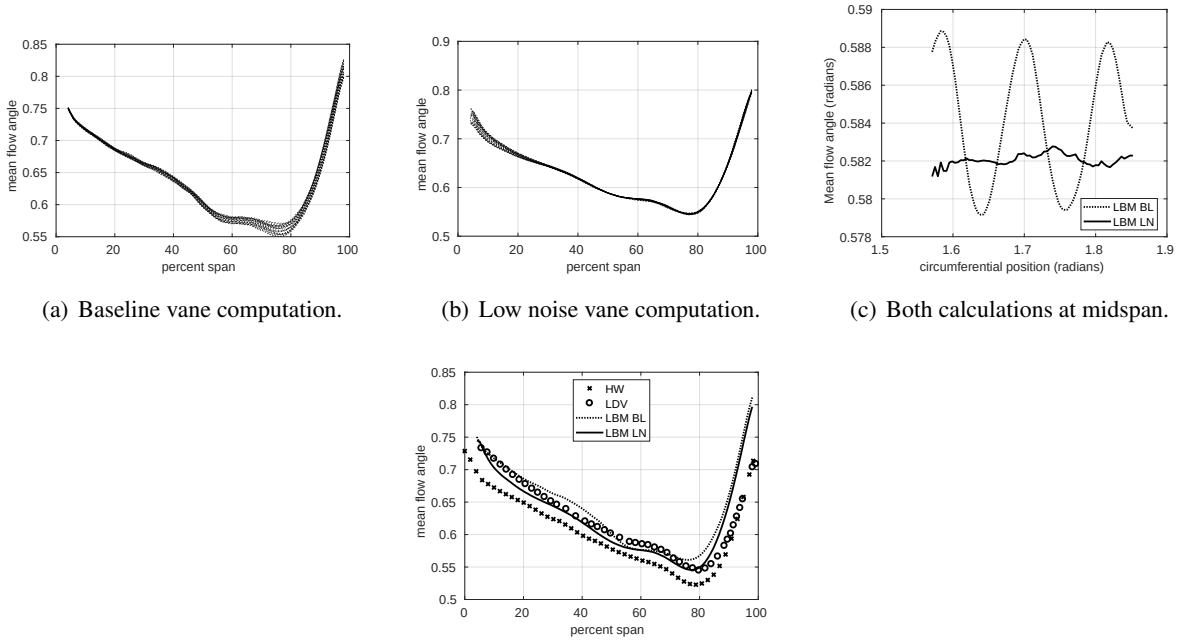

(a) Baseline vane computation.

(b) Low noise vane computation.

(c) Both calculations at midspan.

(d) Comparison.

Figure 9: Mean flow angle at Station 2.

B. Turbulence intensity and TKE

The hotwire and PowerFLOW data are processed identically to obtain the RMS, i.e. turbulence intensity, mean and average passage values. It appears that the simulation that utilizes the turbulent transition trip on the blade surface gives turbulence intensity values closer to those measured with the hot wire. The simulation with a refined grid near the rotor (but the same grid in the wake) leads to lower values of the turbulence intensity. Whether the hot wire results have the same bias as was shown for the mean flow measurements will be addressed in the future. At any given radial position, the turbulence is close to isotropic both in the measurement and in the simulations. The largest deviation is seen in the no trip calculation where the tangential turbulence intensity is significantly smaller than the streamwise and upwash intensities. Additionally, it is clear from the variation in the intensity values with radial position that the turbulence is not homogeneous. The combined turbulence intensity effect is shown in the plot of TKE in Fig. 12.

As was the case for the mean flow, the turbulence intensity does vary depending on where the probes are set circumferentially. An examples of this is shown in Fig. 13. The average passage values of the turbulence intensity at the midspan shown in Fig. 14 have been obtained by averaging over all of the circumferential locations.

The average passage distribution of turbulence intensity again highlights that the wakes that form in the calculation that uses the trip on the blades are too wide. While the wake width from the refined rotor simulation aligns with the measured data. The magnitude of the turbulence in the wake predicted with the refined rotor grid however is low.

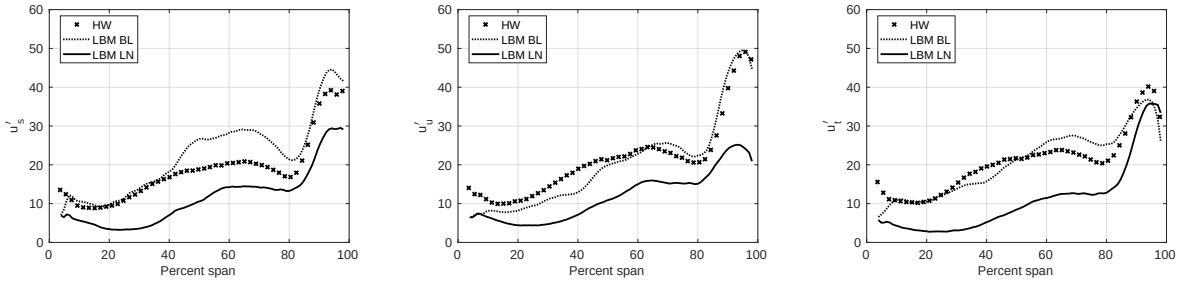

(a) Streamwise (b) Upwash (c) Tangential.

Figure 10: Circumferentially averaged turbulence intensity vs radial location at Station 1.

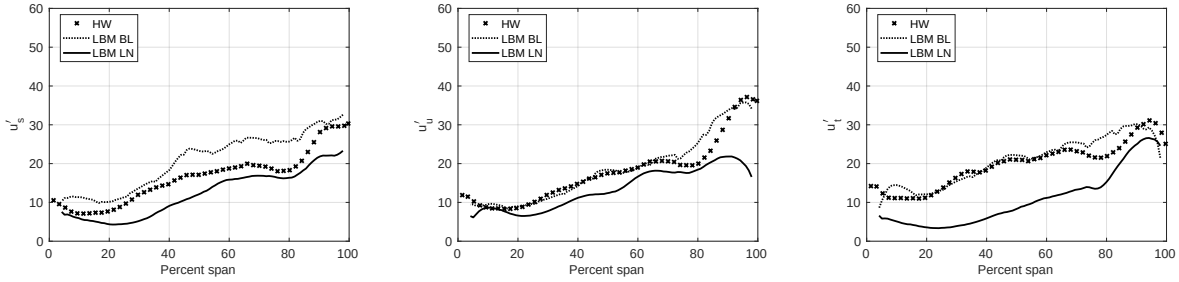

(a) Streamwise (b) Upwash (c) Tangential

Figure 11: Circumferentially averaged turbulence intensity vs radial location at Station 2.

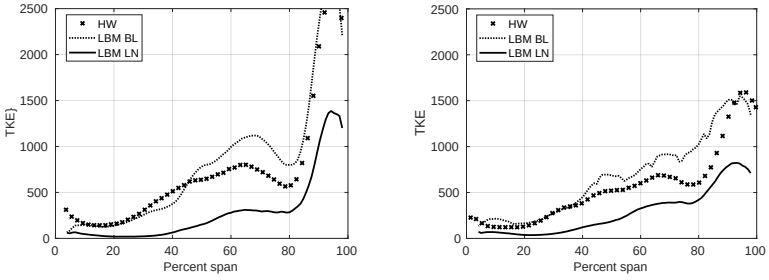

(a) Station 1. (b) Station 2.

Figure 12: Circumferentially averaged turbulence kinetic energy vs radial location.

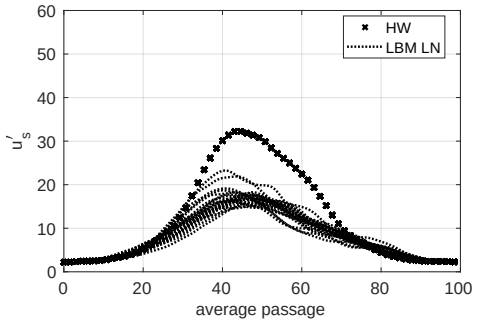

Figure 13: Streamwise turbulence intensity vs radial location for probes at different circumferential locations.

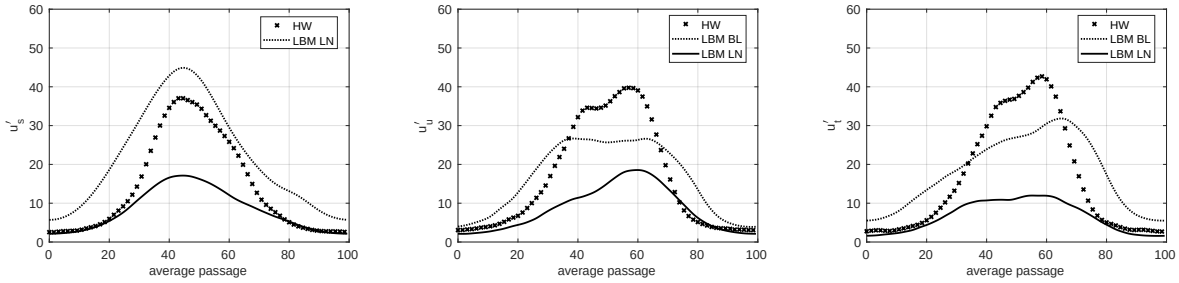

(a) Streamwise (b) Upwash (c) Tangential

Figure 14: Average passage turbulence intensity at midspan at Station 1.

C. Turbulence length scale

The availability of data at virtually any point in the simulations has been used to explore the length scale further than in past studies. First, the stationary probe method for computing the streamwise longitudinal and lateral length scales is shown. As discussion in Section III.B , the calculation relies on Taylor's hy-

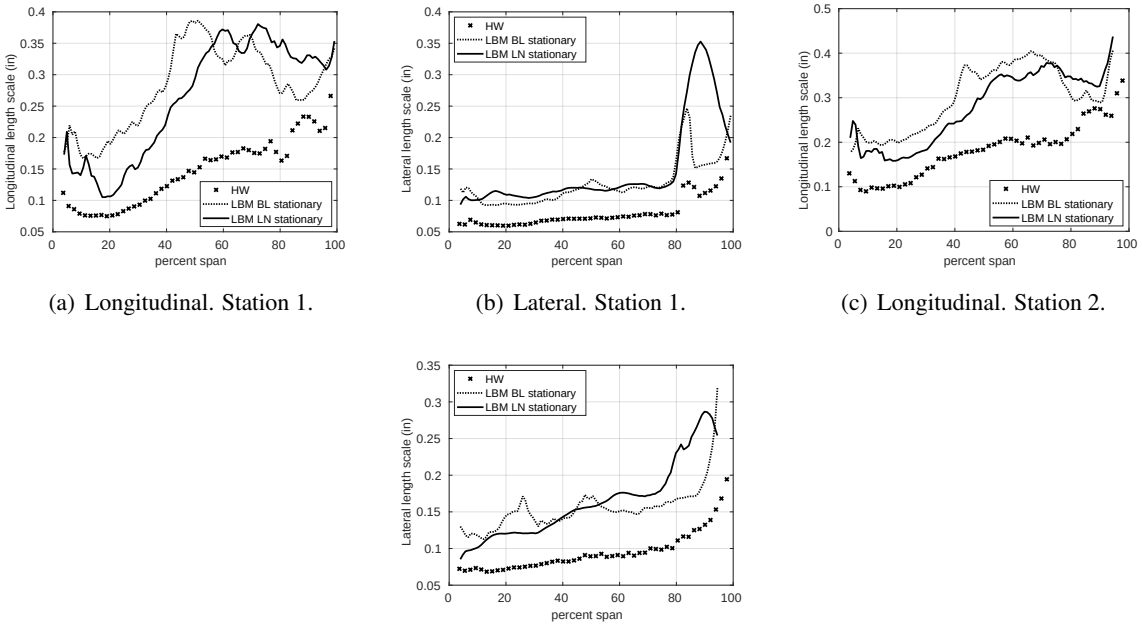

(a) Longitudinal. Station 1.

(b) Lateral. Station 1.

(c) Longitudinal. Station 2.

(d) Lateral. Station 2.

Figure 15: Radial distribution of turbulence length scales computed using stationary method.

pothesis that the disturbance is carried by the meanflow. Figs. 10 and 11 indicate that the turbulence in the rotor wakes only slightly decays as it travels from Station 1 to Station 2. And it is reasonable to assume that the disturbances are carried by the mean flow. The "stationary" length scales computed using Eq. (1) from the fixed probes are shown in Fig. 15. The length scales obtained from the computational data are much larger than those from the experimental data.

The relationship that should hold for isotropic turbulence is that the streamwise longitudinal lengthscale should be double the lateral lengthscale. This holds reasonably well as shown in Fig. 16 with one exception: near the tip region for the computed results obtained using the turbulent transition trip.

The lengths scales were also computed using probes that are separated axially and streamwise. The longitudinal length scale is obtained by considering the flow component in the direction of separation while the lateral length scale is obtained using a flow component per-

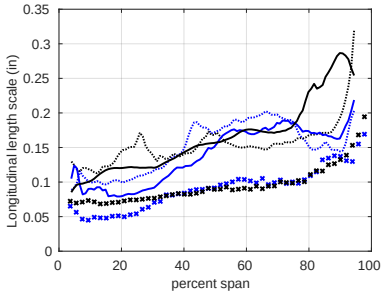

Figure 16: Radial distribution of turbulence length scales at Station 2. Blue lines are one half of the longitudinal length scale. Black lines are the lateral length scale. Line types match those in Fig. 15

pendicular to the direction of separation. The
computation using the axial separation included an average over all of the circumferential locations. The streamwise separation however traverses the entire circumferential extent of the data volume and much of the distance between Stations 1 and 2. Therefore different starting locations in the circumferential direction cannot be used and the calculation must be referenced to an axial position very close to Station 1. As shown in Fig. 4b, when moving between circumferential positions, the mean wake properties change slightly due to grid effects. Therefore it is surmised that the calculation using streamwise separation will be less accurate. Fig. 17 shows the results for longitudinal and lateral length scales computed using streamwise and axial separations. Except near the hub and tip, the lengthscales computed from the computations using the different correlation directions agree relatively well.

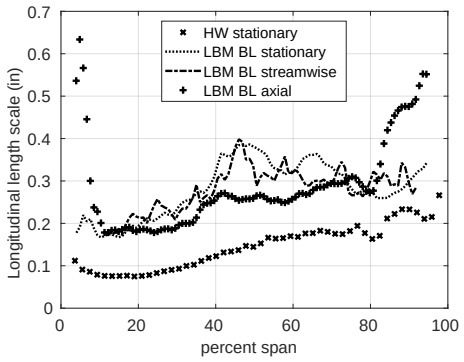

(a) Longitudinal.

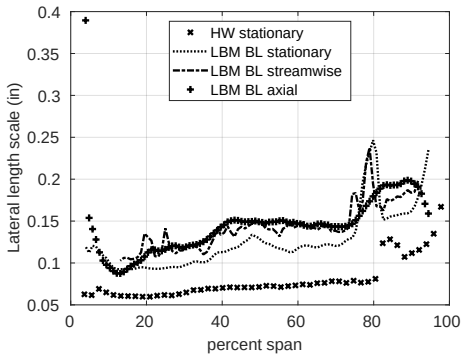

(b) Lateral

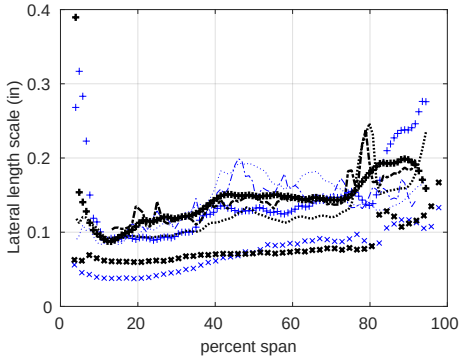

(c) Longitudinal by 1/2 vs. lateral.

Figure 17: Radial distribution of turbulence length scales (Station 1 starting points for the spatial correlations).

Finally, radial separation was considered. It seems that the longitudinal length scale should be able to be computed using either dr separation values that are positive (from hub to tip) or negative (from tip to hub). However, the results do not give the same thing as seen in Fig. 18. The issue may arise from the fact that the direction of the flow is positive from hub to tip and switching the separation direction misaligns it with the flow direction by 180°. However, any separation direction should work for the lateral length scale. For instance, if it is the axial flow direction of interest and the separation is in the radial direction, it should not matter if the separation is considered in an outward or inward sense. However, the same disagreement is

seen for the lateral case as is seen in Fig. 18. This result will be studied more carefully in the future.

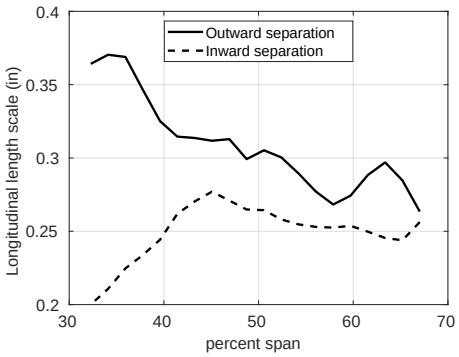

Figure 18: Longitudinal radial length scale at Station 2, computed using outward and inward separation distances.

D. Spectra

The interest in studying the gap flow in detail stems from the dependence of the interaction noise on the inflow to the FEGV. For broadband noise, it is the broadband portion of the inflow turbulence spectrum responsible for the noise. If one utilizes the two-step approach to predicting the noise, then a spectrum is created based on accepted models such as von Karman, Liepmann, or Gauss. Each model describes the three dimensional energy spectrum as defined by

$$\int_0^\infty E(k,t)dk = \frac{3}{2}u'^2 \tag{3}$$

with $k = \sqrt{k_1^2 + k_2^2 + k_3^2}$ being the magnitude of the wave number vector. In the past, the similarity between the von Karman and Liepmann models have been shown and as such only the Liepmann and Gauss are considered in this paper. The models are built using the turbulence intensity and turbulence length scale.

Hinze[11] provides the one-dimensional spectral models as well as the full three-dimensional models. For Liepmann they are given as

$$E_{L1} = \frac{2}{\pi}u'^2\frac{\Lambda}{1+(k_1\Lambda)^2} \tag{4}$$

$$E_{L2} = \frac{1}{\pi}u'^2\Lambda\frac{1+3(k_1\Lambda)^2}{(1+(k_1\Lambda)^2)^2} \tag{5}$$

$$E(k) = \frac{8}{\pi}u'^2\Lambda\frac{(k_1\Lambda)^4}{(1+(k_1\Lambda)^2)^3} \tag{6}$$

where Λ is the longitudinal length scale, and subscripts 1 and 2 refer to the models relation to the longitudinal and lateral correlations respectively. The Gaussian model is given as

$$E_{G1} = \frac{2}{\pi}u'^2\Lambda e^{-(k_1\Lambda)^2/\pi} \tag{7}$$

$$E_{G2} = \frac{2}{\pi}u'^2\Lambda\left(1+\frac{2}{\pi}(k_1\Lambda)^2\right)e^{-(k_1\Lambda)^2/\pi} \tag{8}$$

$$E(k) = \frac{4}{\pi^2}u'^2\Lambda(k_1\Lambda)^4 e^{-(k_1\Lambda)^2/\pi} \tag{9}$$

We consider a stationary probe near the midspan. The power spectral density (PSD) is computed from the FFT of the time signal. Using the Taylor's hypothesis, the streamwise velocity spectrum should compare to the longitudinal 1D spectrum model while the upwash velocity spectrum should be related to the lateral spectrum model. To compare the models above directly to the PSD, the models must be converted from the wave number space to the frequency domain using the Taylor's hypothesis, $dk = \frac{2}{U_s \pi} df$, where U_s is the streamwise mean flow velocity. We focus on the spectrum at Station 2 because of its relevance to the interaction noise produced by the fan stage. Fig. 20 shows the PSD of the streamwise and upwash velocity components computed from the hotwire data and the computed data.

The fits to each of these PSD using the longitudinal and lateral models described above are shown in Fig. 20. The turbulence intensity and lengthscale used in the models was taken directly from the HW or computed data respectively. The Liepmann model tracks the initial roll off of the streamwise velocity spectrum measured by the HW the best. Neither model captures the roll off of the computed spectrum well. A better model for the spectrum will be addressed in the future.

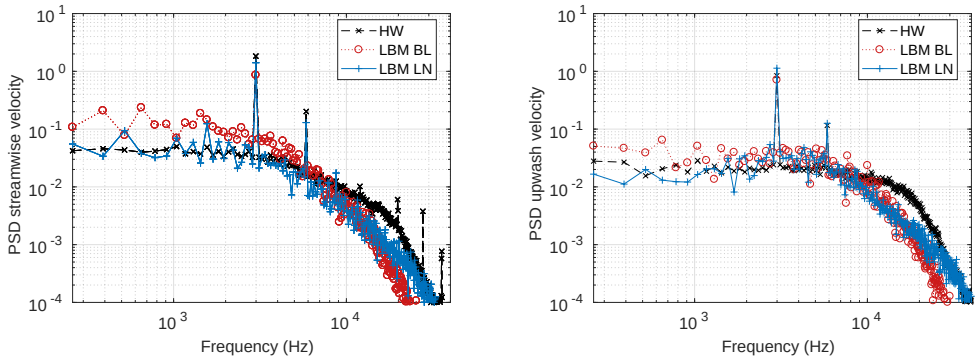

(a) Streamwise.

(b) Upwash.

Figure 19: Power Spectral Density of the velocity at midspan at Station 2.

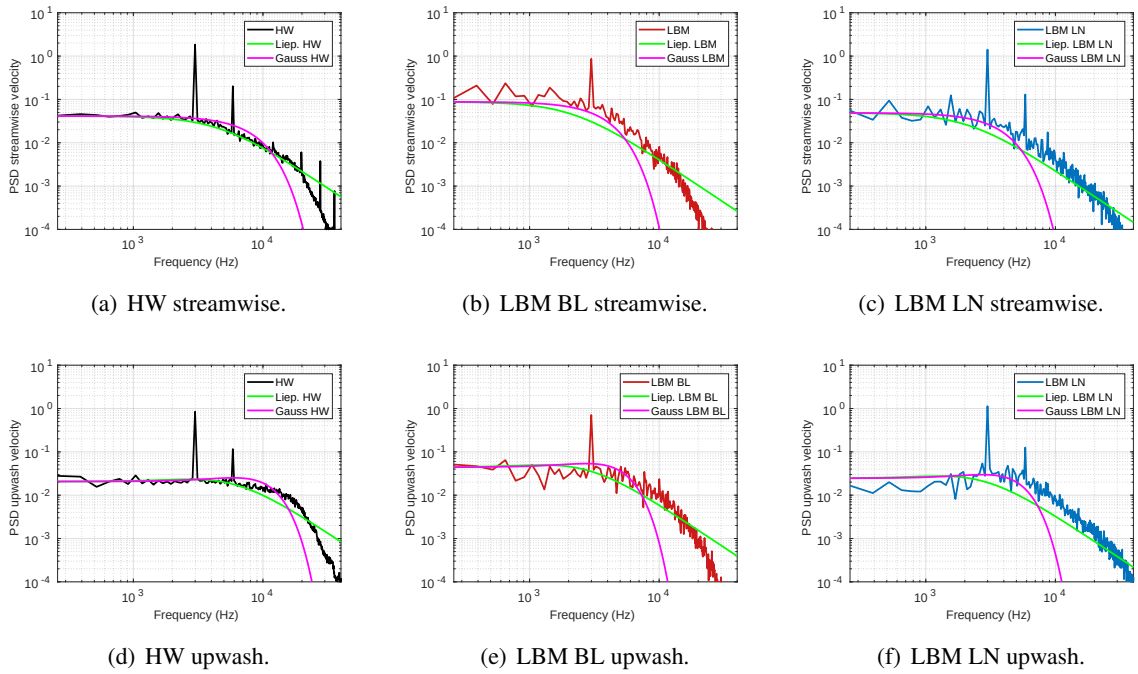

(a) HW streamwise. (b) LBM BL streamwise. (c) LBM LN streamwise.

(d) HW upwash. (e) LBM BL upwash. (f) LBM LN upwash.

Figure 20: Power Spectral Density of the velocity at midspan at Station 2.

E. Impact of gap flow differences on broadband noise prediction

The low-order turbofan broadband prediction method described in Ref. [9] is used with input generated from the hotwire and the PowerFLOW simulations. In particular, the quantities that are utilized are the radial distribution of axial and circumferential mean flow, the radial distribution of the mean upwash turbulence intensity, and the radial distributions of the streamwise longitudinal length scale and the radial transverse (upwash) length scale. The Liepmann spectral model was used. The radial transverse length scale has been previously implemented in two ways. It has been set to 1/2 the longitudinal streamwise length scale as justified in Section C. It has also been determined based on the method introduced by Posson et al.[12]

$$L_{r_u} = \frac{3\pi L_{s_s}}{2\sqrt{1+(k_s L_{s_s})^2}} \frac{(k_s L_{s_s})^2}{1+3(k_s L_{s_s})^2} \tag{10}$$

The results are shown in Fig. 21. In Fig. 21a, two sets of input were created from each of the simulations. The first set used the mean flow, upwash turbulence intensity, and longitudinal stationary length scale determined from the simulations. The second set modified the length scale and used the longitudinal axial length scale in the midspan region and the longitudinal stationary length scale near the hub and tip. This modification stemmed from the fact that the longitudinal axial length scale looked much smoother in the midspan region as seen in Fig. 17a. There is an overall overprediction of the sound power at the exhaust duct using this method. Because the spectral model has a large dependence on Λ, even though the low noise simulations (without the trip) gave much lower turbulence intensity values, it is not obvious in the outcomes. The LBM BL simulation inputs were further modified first, such that the radial length scale was selected as Eq. (10), and then second such that the longitudinal length scale from the HW data was used and the radial length

scale was computed using Eq. (10). The results simply highlight the important role that the length scale plays in the two-step method for computing the interaction noise.

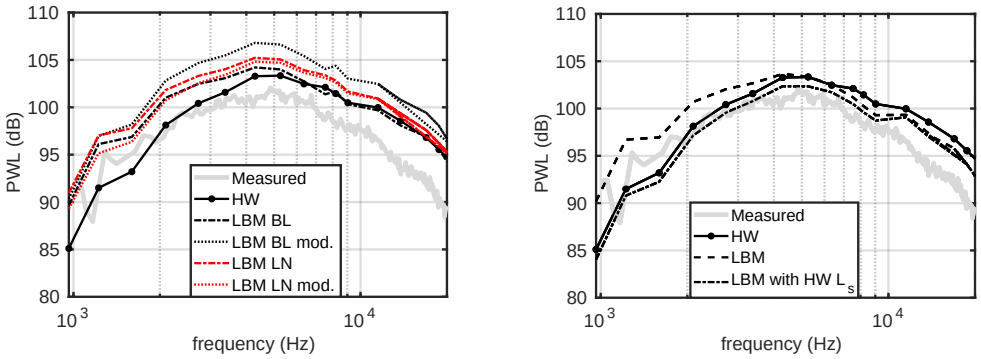

(a) Input fully from LBM.

(b) Radial lengthscale as given in Eq. 10.

Figure 21: Predicted power spectrum at exhaust computing using two-step method. Baseline vane case at approach. Input taken from HW, LBM BL and LBM LN. Switched out lengthscale for that found from HW.

V. Conclusion

The predicted flow in the gap between a fan and FEGV has been investigated. The simulations were performed with the PowerFLOW software that utilizes a VLES computational method. The Source Diagnostic Test configurations provided the cases of interest and comparison experimental data. Simulations of the baseline and low-noise vane configurations were carried out at the approach rotor speed. The baseline vane case was simulated using a turbulent transition trip on the rotor surface. The low-noise vane case used a refined grid near the blade surface and no trip. The mean flow results were shown to be improved by using the refined grid with no trip. Comparison of results from the two simulations show a slight potential effect from the baseline vane on the flow field just upstream of its leading edge. The turbulence intensities predicted by the two simulations are very different; with the tripped case giving higher RMS values. However, both flow simulations show that the turbulence intensity changes only slightly between the mid gap and the vane with the greatest changes coming in the tip region. This supports the rapid distortion theory which assumes that the turbulence is simply convected by the mean flow.

It is shown that the two-step approach to computing the noise generated by the interaction of the fan wake and the FEGV is heavily dependent on the turbulence length scale. As such, a more thorough investigation of the turbulent length scale was undertaken. A stationary method, reliant on Taylor's hypothesis, is used to obtain a length scale from the experimental data. This same approach was used with the computed data. The turbulent length scale determined from the simulated data was found to be much larger than that found from the experimental data. Both simulations predict about the same length scale. Although the values are higher, for both the experimental and computational based length scales, the relationship that the lateral length scale should be one half of the longitudinal length scale was verified. The availability of simultaneously recorded time-resolved data at multiple locations provided an opportunity to further probe the length scale calculation. It was shown that the longitudinal and lateral length scales found using the spatially separated probes were similar to those determined from the stationary method. Length scales computed using radial separation are

dependent upon the direction of separation which is unexplained currently. This will be examined further in the future.

The analysis of the simulation data highlights how challenging it is for computations to resolve the turbulent flow in a fan gap well. However, it also highlights how specific differences (which could be from inaccuracies in a simulation) may not impact significantly the prediction of broadband noise from the system. Because the broadband noise is the culmination of a physical averaging of many effects, acoustic predictions obtained directly from the VLES method or from the two-step method based on the VLES turbulent flow information may in fact still be accurate enough to be useful for engine analysis and design.

VI. Acknowledgments

The past efforts of BU graduate alum Jeremy Maunus, Professor Emeritus Victor Yakhot, and past BU RCS staff member Douglas Sondak are recognized for providing the quantitative assessment method for the interstage turbulent flow. The authors also acknowledge that the data analysis and low-order fan broadband calculations reported in this paper were performed on the Shared Computing Cluster which is administered by Boston University's Research Computing Services. The SDT results belong to the RC1 portfolio of benchmark problems designed to assess the state of the art in fan broadband noise prediction. Further information may be found at http://www.oai.org/aeroacoustics/FBNWorkshop. Ed Envia is acknowledged for his work compiling and distributing the fan broadband workshop geometry and data. Partial support for this work came from a grant from the Aeroacoustics Research Consortium administered by the Ohio Aerospace Institute.

References

[1]Grace, S., Gupta, A., Gonzalez-Martino, I., and Casalino, D., "Statistics and structure of turbulence in a fan/FEGV interstage and their aeroacoustic implications," *AIAA Paper No. AIAA 2018-4186*, 2018, pp. 1–18.

[2]Casalino, D., Hazir, A., and Mann, A., "Turbofan Broadband Noise Prediction using the Lattice Boltzmann Method," *AIAA Journal*, Vol. 56, No. 2, 2018.

[3]Heidelberg, L. J., "Fan Noise Source Diagnostic Test-Tone Modal Structure Results," *AIAA Paper No. 2002-2428*, 2002, 8th AIAA/CEAS Aeroacoustics Conference.

[4]Woodward, R. P., "Fan Noise Source Diagnostic Test-Farfield Acoustic Results," *AIAA Paper No. 2002-2427*, 2002, pp. 1–12., doi : 10.2514/6.2002-2427.

[5]Envia, E., "Fan Noise Source Diagnostic Test-Vane Unsteady Pressure Results." *AIAA Paper No. 2002-2430*, 2002, 8th AIAA/CEAS Aeroacoustics Conference.

[6]Envia, E., c. Hughes, Podboy, G., and Woodward, R., "Fan Noise Souce Diagnostic Test Completed and Documented," Tech. Rep. TM-2005-0214860, NASA, 2003.

[7]Maunus, J., Grace, S. M., Sondak, D. L., and Yakhot, V., "Characteristics of Turbulence in a Turbofan Stage," *Journal of Turbomachinery*, Vol. 135, No. 2, March 2013, pp. 021024–1–10.

[8]Maunus, J., Grace, S. M., and Sondak, D. L., "Effect of Rotor Wake Structure on Fan Interaction Noise," *AIAA Journal*, Vol. 50, No. 4, April 2012, pp. 818–831.

[9]Grace, S., "Fan Broadband Interaction Noise Modeling Using a Low-Order Method," *Journal of Sound and Vibration*, Vol. 346, 2015, pp. 402–423.

[10]Podboy, G. G., Krupar, M. J., Helland, S. M., and Hughes, C., "Steady and Unsteady Flow Field Measurements Within a NASA 22-Inch Fan Model," Tech. Rep. TM-2003-212329, NASA, 2003.

[11]Hinze, J. O., *Turbulence*, McGraw-Hill International Book Co., New York, etc., 1975.

[12]Posson, H., Moreau, S., and Roger, M., "Broadband noise prediction of fan outlet guide vane using a cascade response function," *Journal of Sound and Vibration*, Vol. 330, 2011, pp. 6153–6183.